IOP Publishing Journal of Physics: Condensed Matter
J. Phys.: Condens. Matter **27** (2015) 175001 (9pp) doi:10.1088/0953-8984/27/17/175001

Structural analysis of strained $LaVO_3$ thin films

H Rotella[1,5], O Copie[1,6], G Steciuk[1], H Ouerdane[1,7], P Boullay[1], P Roussel[2], M Morales[3], A David[1], A Pautrat[1], B Mercey[1], L Lutterotti[4], D Chateigner[1] and W Prellier[1]

[1] Laboratoire CRISMAT, UMR 6508 CNRS, ENSICAEN et Université de Caen Basse Normandie, 6 Boulevard Maréchal Juin, F-14050 Caen, France
[2] Laboratoire UCCS, CNRS UMR 8181, ENSCL, Bat C7, BP 90108 F-59652 Villeneuve d'Ascq, France
[3] Laboratoire CIMAP, CNRS UMR 6252, ENSICAEN et Université de Caen Basse Normandie, 6 Boulevard Maréchal Juin, F-14050 Caen, France
[4] Dipartimento di Ingegneria Industriale, Univ. di Trento, 9 via Sommarive, 38123 Trento, Italy

E-mail: philippe.boullay@ensicaen.fr

Received 19 December 2014, revised 6 February 2015
Accepted for publication 13 February 2015
Published 13 March 2015

Abstract

While structure refinement is routinely achieved for simple bulk materials, the accurate structural determination still poses challenges for thin films due on the one hand to the small amount of material deposited on the thicker substrate and, on the other hand, to the intricate epitaxial relationships that substantially complicate standard x-ray diffraction analysis. Using both electron and x-ray diffraction, we analyze the crystal structure of epitaxial $LaVO_3$ thin films grown on (1 0 0)-oriented $SrTiO_3$. Transmission electron microscopy study reveals that the thin films are epitaxially grown on $SrTiO_3$ and points to the presence of 90° oriented domains. The mapping of the reciprocal space obtained by high resolution x-ray diffraction permits refinement of the lattice parameters. We finally deduce that strain accommodation imposes a monoclinic structure onto the $LaVO_3$ film. The reciprocal space maps are numerically processed and the extracted data computed to refine the atomic positions, which are compared to those obtained using precession electron diffraction tomography.

Keywords: thin films, crystallography, strained layers, electron microscopy, x-ray diffraction

(Some figures may appear in colour only in the online journal)

1. Introduction

Transition metal oxides (TMOs) derived from the perovskite structure form a class of materials that exhibits a broad spectra of functional properties such as metal–insulator transition, ferroelectricity, superconductivity, and colossal magnetoresistance [1, 2]. They originate from the particular electronic and atomic structures of perovskite, which induce high electronic polarizability and strong Coulomb correlations; and unlike conventional semiconductors or metal, there is no dominant mechanism that dictates their macroscopic properties. Amongst the interactions that give rise to strong coupling between lattice, electric charges, spins and orbitals, all compete with comparable strength in these systems. For instance, octahedral rotations in ABO_3 perovskite may strongly affect magnetic and transport properties through the modification of the B–O–B angles affecting the orbital overlaps. The majority of the perovskite compounds are distorted derivatives of the parent cubic ($Pm\bar{3}m$ (#221)) resulting from a combination of the following contributions: (i) tilting of BO_6 octahedra; (ii) Jahn–Teller distortion of BO_6 octahedra; (iii) shearing of BO_6 octahedra; (iv) cation displacement. Several theoretical studies have already addressed the crucial role of these contributions on electronic

[5] Present address: CEA, LETI, Minatec, 17 rue des martyrs, F-38054 Grenoble, France.
[6] Present address: Service de Physique de l'Etat Condensé, DSM/IRAMIS/SPEC CNRS UMR 3680 CEA Saclay, F-91191 Gif sur Yvette, France.
[7] Present address: Russian Quantum Center, Business center Ural, 100A, Novoya street, Skolkovo, Moscow 143025, Russia.

 © 2015 IOP Publishing Ltd Printed in the UK

properties [3]. Correlatively, these materials are very sensitive to external constraints such as temperature or hydrostatic pressure. Taking advantage of the substrate-induced biaxial strain, the thin film deposition provides a convenient way to tune their properties [3–7]. Many progresses have been made in the synthesis of perovskite thin films and complex heterostructures but a fine analysis of their crystal structures is still missing. As the control of the properties in these systems is important in view of their potential applications, it is crucial to get access to reliable cell parameters and atomic positions on materials deposited in the form of thin films.

X-ray diffraction (XRD) is the most widely used non-destructive analytical technique to access relevant informations on a crystal structure. However, in case of a thin film epitaxially grown on a substrate, the geometry of the sample and the small diffracting volume strongly reduce the interest of this technique. First, the epitaxy of the film produces a highly textured material which often presents oriented crystallographic domains, resulting in a complex diffracted pattern with the convolution of several crystallographic planes contribution in one particular reflection. Second, the amount of substrate material being about 10^3 times larger than that of the film, the diffracted beam coming from the substrate is much more intense than the film signal. If the structures are close, the deconvolution of the two signals becomes difficult. Third, as the small diffracting volume of the film produces a weak diffracted beam, this may result in the apparent extinction of the weak reflections in the diffracted patterns which should normally be present because of the peculiar film structure. In addition to those sample constraints, the experimental set-up itself produces limitations in the data acquisition: the system, film and substrate, only allows the reflection configuration. In this specific configuration, the experimental set-up produces shadow zones in the diffracted pattern, resulting in inaccessible reflections [8]. In this work, we will show how these drawbacks can be partially bypass with a structure analysis that separately focus on the film/substrate epitaxial relations and on the film lattice parameters refinement. Note that even the determination of the atomic positions can be made separately by focusing on a particular species of atoms. In the case of oxide perovskite compounds, it is known that the displacements of the oxygen atoms from their ideal positions produce specific reflections in the diffracted pattern [9, 10]. Using XRD, partial structural studies focused on the determination of the amplitude of octahedral tiltings in thin films were already achieved [11–15].

Regarding structure determination of unknown phases deposited in the form of thin films, precession electron diffraction (PED) [16] has proved to be one valuable technique [17, 18] not limited by the size of the probe nor the small volume of diffracting material. We will illustrate here how PED can afford a valuable complement to XRD in the structural analysis of a $LaVO_3$ (LVO) thin films grown on (0 0 1)-oriented $SrTiO_3$ (STO) substrates. In its bulk form, LVO crystallizes at room temperature in an orthorhombic structure (Pnma (#62)) with the following lattice parameters, $a_o = 5.55548(4)$ Å, $b_o = 7.84868(6)$ Å and $c_o = 5.55349(5)$ Å [19]. The LVO structure presents tilting of BO_6 octahedra and La displacements which makes it a derivate of the parent cubic structure ($Pm\bar{3}m$ (#221)) adopted by STO. In the case of bulk LVO these distortions are relatively small and the lattice parameters can be related to a pseudocubic structure according to the following equation: $a_p \simeq a_o/\sqrt{2} \simeq b_o/2 \simeq c_o/\sqrt{2} \simeq 3.9251(1)$ Å. The expected mismatch between $a_{p-\mathrm{LVO}}$ and a_{STO} is about 0.5% indicating a film compressive stress. This case study gathers some of the problematics that occur typically on oxide perovskite thin films and, more generally, on any epitaxial thin film. First, we will present an in-depth study of the structure of LVO thin films using XRD and precession electron diffraction tomography (PEDT) [20]. Second, we will discuss the obtained results by our approach as a promising thin film structure determination for complex systems.

2. Experimental

Epitaxial $LaVO_3$ (LVO) thin films were grown by pulsed laser deposition technique on (0 0 1)-oriented $SrTiO_3$ (STO) substrate (cubic $a = 3.905$ Å). To grow the films, a KrF laser ($\lambda = 248$ nm) with a repetition rate of 2 Hz and a fluence of $\simeq 2\,\mathrm{J\,cm^{-2}}$ was focused onto a $LaVO_4$ polycrystalline target. The substrate was kept at 700 °C under a dynamic vacuum near 10^{-5} mbar. The distance between the target and the substrate is 8.5 cm [21, 22].

The sample used for transmission electron microscopy (TEM) analysis was prepared in cross-section using a JEOL ion slicer. After a hand polishing with a series of grinding paper, the cross-section was finished by using an Ar ion beam to decrease the thickness down to electron transparency. High resolution electron microscopy (HREM) images were obtained using a FEI Tecnai G2 30 (LaB6 cathode) microscope. Precession Electron Diffraction tomography data were recorded on a JEOL 2010 (LaB6 cathode) microscope equipped with a Nanomegas DigiStar precession module and an upper-mounted Gatan Orius CCD camera. 64 PED patterns were recorded in the tilt range −33 to +30 degrees with a precession angle of 1.5 degree. The data analysis and reduction were performed using the programs PETS [23] and Jana2006 [24] following a procedure similar to the one described in [25].

The reciprocal space maps (RSM) were acquired using a high resolution 7-circles Rigaku SmartLab diffractometer having a copper rotating anode ($\lambda = 1.540\,56$ Å) and a 1D detector of 2°. This apparatus presents weak wavelength dispersion ($\Delta\lambda/\lambda = 3.8 \times 10^{-4}$) and weak beam divergence ($\Delta\omega = 32'$). After a classical optimization of the diffractometer angles on the substrate, for intensity measurements of the film, the angles were adjusted to maximize the film intensity. We scanned a total of 26 RSMs either in coplanar or non-coplanar configurations. Using the proper slits for the 1D detector (1 × 1 mm), the resolution of coplanar RSM is comparable than the one obtained using a crystal analyzer and the detector in 0D mode (point detector).

The sample reference frame (figure 1) used in the RSM corresponds to $\vec{x}$ and $\vec{y}$ axes aligned with the main edges of the sample, and $\vec{z}$ perpendicular to the sample surface. The diffractometer rotation axes are the conventional χ (tilt),

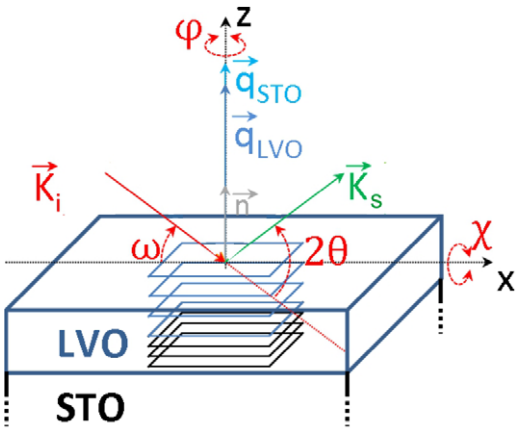

Figure 1. Schematic representation of the measurement configuration and definition of the sample reference coordinate systems. $\vec{k}_i$ and $\vec{k}_s$ represent, respectively, the incident and scattered beam vectors.

ω (incident) and ϕ (azimuth) angles, with the incident x-ray beams at ω from the sample plane at $\chi = 0$, and its projection on the sample plane aligned with the $\vec{x}$ axis at $\phi = 0$. The fourth circle of the diffractometer corresponds to the Bragg angle, 2θ, given by the detector position.

When rotating the sample around χ, ω and ϕ, the beam penetrates the sample in different ways, and, as shown in the following equations, a correction of the diffracted intensity at each (χ, ω, ϕ, θ) measured point becomes necessary [26] before analysis:

$$I_{\text{corr}} = \frac{I_{\text{mes}}}{A_{\chi}^{\text{film}}} \tag{1}$$

where A_{χ}^{film} is the correction factor:

$$A_{\chi}^{\text{film}} = \frac{2}{\sin 2\theta M(\omega, 2\theta)} \frac{1 - \exp\left[\frac{-\mu T M(\omega,2\theta)}{\cos\chi}\right]}{1 - \exp\left[\frac{-2\mu T}{\sin 2\theta \cos\chi}\right]} \tag{2}$$

with T the effective thickness of the sample and

$$M(\omega, 2\theta) = \frac{1}{\sin 2\theta} + \frac{1}{\sin(2\omega - 2\theta)}. \tag{3}$$

Once this correction is applied, we process the corrected RSM. Each RSM is made of a series of 1D diffractograms with 2° intervals in ω for one fixed 2θ. To calculate the integrated intensity of each RSM, we developed a program that fits each (ω,2θ) scan (figure 2).

3. Results and discussion

Preliminary investigations were made by TEM on a 200 nm-thick film. The TEM bright field image obtained along one $< 1\,0\,0 >_{\text{STO}}$ direction (figure 3(*a*)) presents a high crystalline quality with a perfect epitaxy of the film on the substrate. In the whole thickness, the film is made of 90°-oriented nanosized domains as evidenced by HREM imaging (figure 3(*b*)) and selected area electron diffraction (SAED) patterns (figure 3(*c*)). In this pattern, the most intense reflections correspond to the perovskite subcell common to both STO and LVO phases and are indicated by black dots in the schematic figure 3(*d*). The weak reflections denote the presence of a superstructure as referred to the $Pm\bar{3}m$ prototype perovskite. They can be indexed if one considers that the LVO film presents a distorted perovskite structure involving rotation of VO_6 octahedra consistent with the ones existing in bulk LVO [19]. In this case, considering the existence of 90° oriented domains, the weak reflections can be separated in two subsets associated, respectively, to [0 1 0] and [1 0 1] zone axes patterns of a Pnma structure having cell parameters $a_p\sqrt{2}\times 2a_p \times a_p\sqrt{2}$. In figure 3(*e*), these two orientations correspond to the case where the *b*-axis of the Pnma LVO structure is parallel to the substrate plane but differs by an in-plane rotation of 90° around $\vec{z}$. Considering its Pnma bulk form, the epitaxial relationship for LVO can be written as (1 0 1)LVO‖(0 0 1)STO with for LVO_I: [0 1 0]LVO‖[1 0 0]STO and for LVO_{II}: [0 1 0]LVO‖[0 1 0]STO. Interestingly, the microstructure of LVO deposited in this 200 nm thick film offers strong similarities with the one observed for thin LVO layers in LVO/$SrVO_3$ heterostructures [27].

A perfect epitaxial film, without any growth defects nor orientation domains i.e. a single crystal would behave like a perfectly textured sample with one orientation component. However, most of the epitaxial thin films are composed of several crystallites with different orientations. In the case of our LVO thin film, according to the TEM analysis, four 90° oriented domains are present in the sample i.e. the two represented in figure 3(*e*) plus their equivalents by a 180° in plane rotation around $\vec{z}$. In order to get a better view on how these oriented domains shall affect the RSM measured by XRD, the simulation of the expected pole figures, represented in equal area projections [26], were performed with the MAUD software [28] considering the bulk LVO structure [19]. For simplicity, we focus only on the 101, 020, 204 and 323 reflections. First, considering that the film is fully textured, i.e. with only one orientation component, we simulate the four pole figures (figure 4(*a*)). Each pole, as well as its multiplicity, is clearly observed independently from the others. Second, the four 90° oriented domains of the film are considered for the simulations (figure 4(*b*)). The convolution of several poles appears at the same location in the pole sphere. At the equator of the pole sphere, the 101 and the 020 equivalents are mixed; so do the 204 and 323 equivalents near the north pole. Following the TEM observations, these simulations indicate that the presence of 90°-oriented domains implies that some reflections present the contributions of several crystallographic planes.

To further investigate the structure of LVO in a thin film form, we performed high resolution XRD measurements on a 100 nm thick film. First, we focused on the characterization of the epitaxial relationships between the film and the substrate examining the four asymmetric reflections (204), (402), (323) and (3-23) shown in figure 5. In coplanar geometry, in order to plot the RSM maps, the angles made by the incident beam with respect to the sample surface (ω) and the angle made by the scattered beam with respect to the incident beam (2θ) are usually converted into reciprocal lattice units with $q_x = \frac{2\pi}{\lambda}[\cos(2\theta - \omega) - \cos\omega]$ and $q_z = \frac{2\pi}{\lambda}[\sin(2\theta - \omega) + \sin\omega]$.

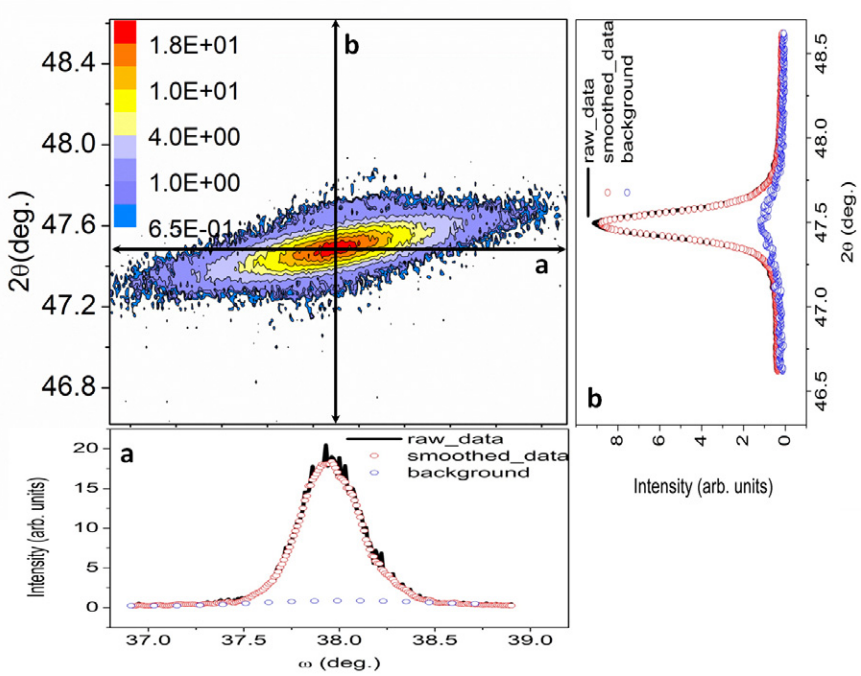

Figure 2. (2 1 2) Reciprocal space map of LVO. The raw and smoothed data, with the associated background, for a ω scan at a given 2θ value (represented by the a arrow) is plotted in (a). The distribution of the intensity of the smoothed data and the background along 2θ represented by the (b) arrow and plotted in (b).

The RSM (figure 5) shows that the LVO film is coherently and fully strained on the substrate, i.e. we observe a perfect vertical alignment between both families of reflections from film and substrate. As expected from the pole figure simulations (figure 4(b)), the horizontal alignment of these four reflections reveals that they are equivalent due to the presence of oriented domains in the film. We can conclude from this observation that the a_p and b_p lattice parameters of LVO thin film are qualitatively very close. Also, the relative fractions of the four 90° oriented domains are equal, with equivalent measured intensity for the four groups of reflections. This is in agreement with the TEM observations described above.

To perform cell parameters refinement, we recorded all the accessible reflections allowed by the diffractometer set-up (table 1). Unfortunately, we observe a large distortion of the beam imprint with sample tilts (when χ is nonzero). This effect yields an important error on the absolute value in 2θ of the RSM ellipse center explaining why certain reflections in table 1 are not associated with a 2θ position. This can be corrected by using a crystal analyzer placed in front of the detector but cost a decrease of intensity by 2 orders of magnitude. Consequently, several reflections coming from the film could not be reached.

From the list of absolute 2θ positions, we refined the cell parameters of the LVO thin film using the CELREF software [29]. We showed in a previous work that a LVO thin film grown on $SrTiO_3$ has a distorted structure towards monoclinic symmetry [13]. According to group-subgroup relation, the symmetry lowering form orthorhombic to monoclinic with the appearance of a β angle would lead to the space group $P2_1/m$ [30] (most symmetric choice). Thus, the refinement procedure was done using $P2_1/m$ leading to the lattice parameters $a = 5.554(3)$ Å , $b = 7.810(4)$ Å and $c = 5.555(5)$ Å with the monoclinic angle $\beta = 89.45(9)°$ (table 2). The b parameter verifies the relation $b = 7.810(4)$ Å $= 2 \times 3.905$ Å , confirming that the film is fully strained. This quantitative result obtained by the analysis of all accessible reflections is more accurate that the previous qualitative observations [13]. Comparing the bulk values with the refined ones, the a and c parameters remain equal to those of the bulk within our experimental accuracy. But in order to accommodate the substrate strain along $[1\,0\,\bar{1}]$ and $[\bar{1}\,0\,1]$ directions, the angle β becomes smaller than 90°, whereas the b parameter changes significantly. The strain is evaluated to be $\epsilon_2 = (b_B - b)/b_B = 0.5\%$, where b_B is the bulk parameter.

Let us now consider the possibility to refine the atomic positions using the intensities integrated from the RSMs. Some questions might occur regarding the intensities recorded in a non-coplanar configuration ($\chi \neq 0$) for which some distortion of the diffracted beam is observed. In order to retain as many reflections as possible, we assume that the integrated intensity is not influenced by the distortion of the beam when tilting the sample provided the beam imprint stick within the sample surface. Thus, the RSM in coplanar and non-coplanar configurations are investigated to get the maximum number of reflections. Nonetheless, in order to keep the incident intensity on the sample as constant as possible independently of the orientation of the sample, reflections with small ω and high χ values were not measured. Likewise, in our integration process, the errors on the measured reflections are not known and in the following structure refinement we consider a unit weight ponderation scheme to account equitably for all reflections, even the weakest.

While a close analysis of the RSM obtained by XRD evidences a monoclinic distortion of the LVO lattice, the

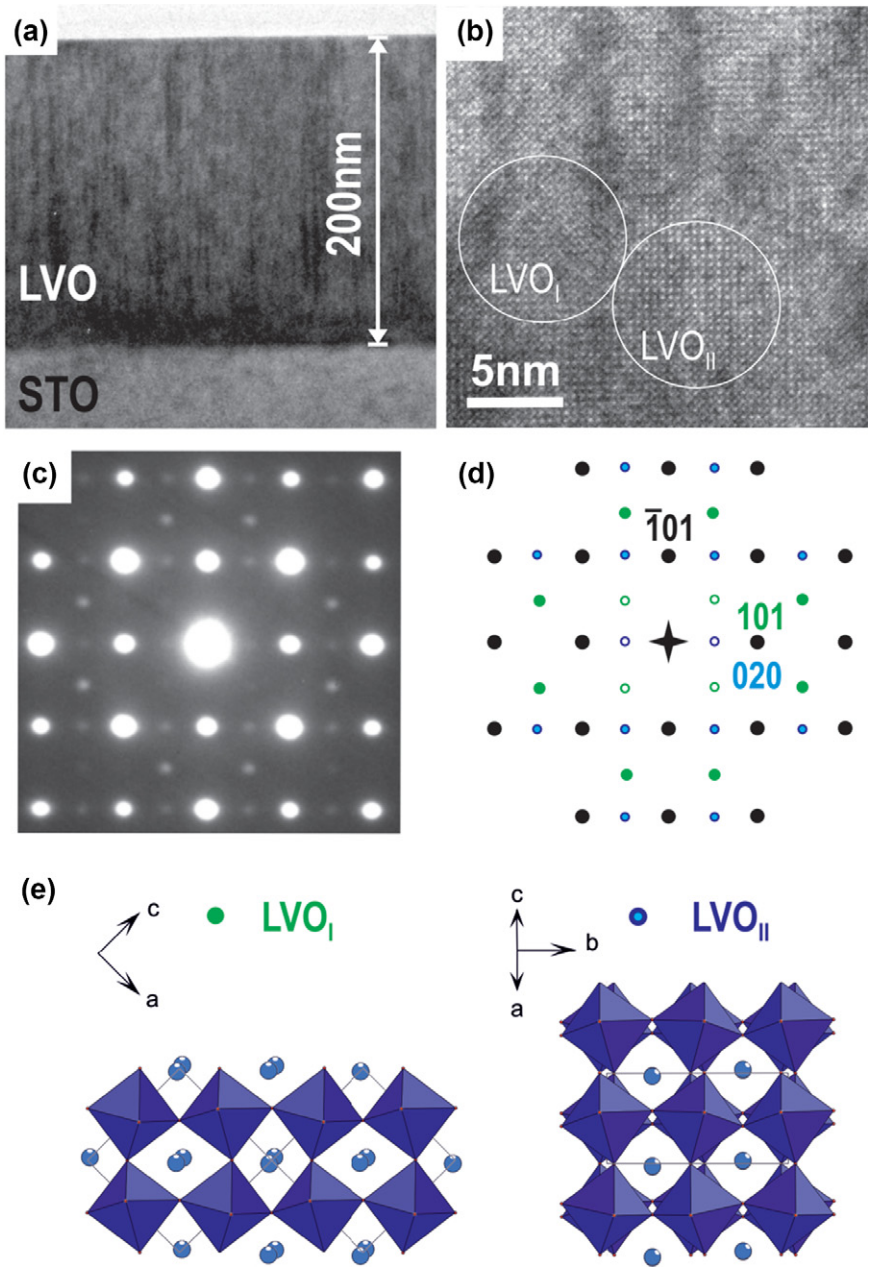

Figure 3. (*a*) TEM bright field view and (*b*) HREM image of a LVO thin film grown on a (0 0 1)-oriented $SrTiO_3$ substrate. (*c*) SAED patterns obtained from an area corresponding to the whole film thickness. (*d*) schematic indexing of the SAED patterns with the contribution of 90°-oriented domains (SG: Pnma) represented in (*e*). Black spots correspond to reflections common to both orientations (perovskite subcell). Reflections specifically related to LVO_I and LVO_{II} are indicated, respectively, in green and blue. The empty symbols represent the forbidden reflexions in the diffracted pattern.

indexing of the 26 measured reflections follows the rules $0kl$: $k+l = 2n$ and $hk0$: $h = 2n$ compatible with the orthorhombic space group Pnma. This is also in agreement with SAED patterns (figure 3). While XRD indicates a weak monoclinic distortion in the metric of the cell, the reciprocal space explored by XRD and SAED exhibits a landscape very similar to orthorhombic Pnma. In the following we thus consider that the LVO thin film structure shall deviate only slightly to an orthorhombic Pnma structure, leading to a number of 7 atomic parameters to refine (see table 3). This number alone is already too high considering that 10 observed reflections per parameter are usually recommended, without considering the scale factor and the atomic displacement parameters (ADP). Nevertheless, considering a global and isotropic value for the ADP and adding the orientation variants with an equivalent volume fraction, the atomic positions plus the scale factor were refined with JANA2006 [24]. In the refinement process, to maintain a reasonable geometry of the O_6-octahedra, we imposed soft constraints on O–O distances to keep them in the same average value as the ones observed in bulk LVO:2.8 Å ± 0.1 Å [19]. Considering this, we obtained the atomic positions indicated in table 3 with reliability factors (Robs and wRobs) around 9%.

In contrast to XRD, the PEDT data collection allowed to access a much larger number of reflections but with the

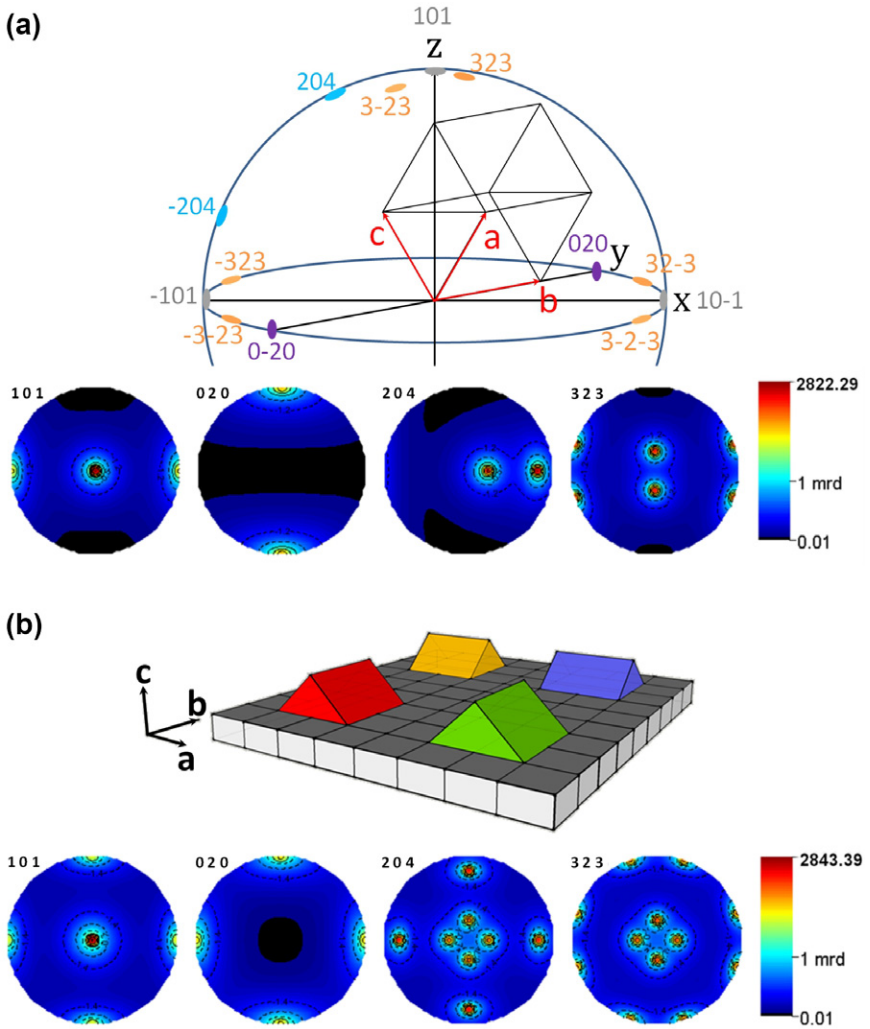

Figure 4. (*a*) (Upper) schematic representation of the pole sphere for a perfect epitaxial thin film of LVO. (Lower) corresponding 101, 020, 204 and 323 pole figures. (*b*) (Upper) schematic representation of the four 90° oriented domains. (Lower) corresponding 101, 020, 204 and 323 directions. Each component is represented as a 10° HWHM Gaussian contribution.

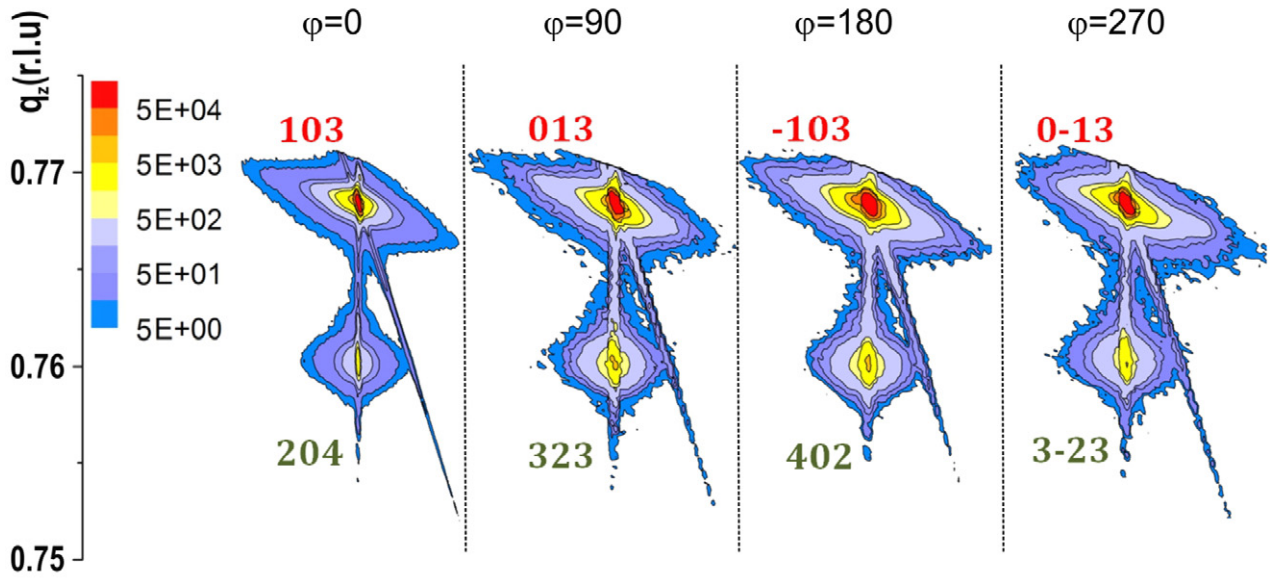

Figure 5. Reciprocal space maps along the $< 103 >^*$ $SrTiO_3$ and [204]*, [402]*, [323]*, [3-23]* of LVO directions. The horizontal axis is q_x for each of the 4 RSMs.

Table 1. 2θ positions and integrated intensities of the measured reflections.

$h\,k\,l$	$2\theta(^\circ)$	I_{int}	$h\,k\,l$	$2\theta(^\circ)$	I_{int}
1 0 1	22.52(1)	118	0 3 3		0.012
1 0 2		0.016	3 3 1	63.82(1)	0.56
2 1 1		0.610	4 0 0		60
2 2 1		0.027			
2 0 2	45.97(1)	500	4 1 0		0.67
0 4 0	46.47(1)		4 0 1	69.59(1)	0.011
2 1 2	47.48(1)	1.65	4 1 1	70.77(1)	0.046
2 3 1		0.14	3 0 3	71.67(1)	2.5
1 3 2		0.14	3 1 3	72.83(1)	0.93
1 0 3		27	4 2 1	74.32(1)	
3 1 1	53.34(1)	0.77	2 0 4	76.31(1)	78
1 2 3	57.42(1)	151	3 2 3	76.32(1)	77
2 0 3	59.70(1)	0.008	3 $\bar{2}$ 3	76.31(1)	78
3 1 2	61.00(1)	0.016	4 0 2	76.31(1)	79

Note: Neither the 2θ positions of the non-coplanar reflection measured without analyzer, nor the integrated intensity of both 040 and 421 (different set-up configuration for the 040 and too much distortion on the 421), are reported.

Table 2. Cell parameters refined for our LVO thin film deposited on STO.

	Bordet *et al* [19]	This work
a	5.555 48(4) Å	5.554(3) Å
b	7.848 68(6) Å	7.810(4) Å
c	5.553 49(5) Å	5.555(5) Å
α	90.0°	90.0°
β	90.0°	89.45(9)°
γ	90.0°	90.0°

drawback of being a destructive method and the necessity to prepare a cross-section of the film. Hence, about 3000 reflections were measured leading to 160 unique reflections (averaged from 1750 reflections observed with $I > 3\sigma(I)$). The structure was refined using both Pnma and $P2_1/m$ space groups (without O–O distance constraints for Pnma and with O–O constraints in the case of $P2_1/m$) (table 3). The PED data are biased by dynamical scattering effects still present even using the precession method and the values of the reliability factors (Robs and wRobs around 19%) are typical of the ones obtained for a refinement against PED data considering the kinematical approximation. Looking at figure 6, both Pnma and $P2_1/m$ refinements give very similar results.

For the various reasons detailled previously, the refinements give reliability factors higher than the standards usually required in crystallography. Correlatively, the obtained atomic positions (table 3) and interatomic distances (table 4) have to be taken with caution especially for the refinement against XRD where the uncertainties on atomic positions and distances are comparatively large. When comparing the structures represented in figure 6, the octahedral tilting directions and amplitudes look similar between the bulk and the PEDT refinements but differs in amplitude with the XRD refinement. This last refinement clearly lacks of sensitivity regarding oxygen atomic positions which are not accurate enough to draw valuable conclusion. The most noticeable difference between the bulk and the thin films structure actually

Table 3. Results of the refinement of LVO thin films using XRD and PEDT data. The structure of the bulk LVO is given as a reference. The refinement were done with the cell parameters $a = 5.554$ Å, $b = 7.810$ Å and $c = 5.555$ Å in both Pnma and $P2_1/m$ space group with $\beta = 89.45$ in the case of $P2_1/m$. In the XRD refinement, isotropic thermal displacement parameters (Uiso) were refined to an overall value for all the atomic positions. The reliability factors Robs/wRobs are 9.4/8.1, 18.2/20.9 and 14.9/16.1, respectively, for the XRD, PEDT(Pnma) and PEDT($P2_1/m$) refinement.

atom	x	y	z	Uiso(Å^2)
		Bulk reference [19]		
La1	0.0295(4)	0.25	0.9951(8)	
V1	0.5	0	0	
O1	0.4880(6)	0.25	0.0707(10)	
O2	0.2831(6)	0.0387(4)	0.7168(6)	
		Thin film (XRD Pnma)		
La1	0.007(2)	0.25	0.001(3)	0.065(6)
V1	0.5	0	0	—
O1	0.503(15)	0.25	0.03(2)	—
O2	0.262(14)	0.014(12)	0.742(15)	—
		Thin film (PEDT Pnma)		
La1	0.0127(6)	0.25	0.9965(8)	0.018(2)
V1	0.5	0	0	0.023(3)
O1	0.499(4)	0.25	0.052(4)	0.021(6)
O2	0.272(3)	0.039(6)	0.730(3)	0.027(5)
		Thin film (PEDT $P2_1/m$)		
La1	0.0006(7)	0.25	0.9878(7)	0.020(2)
La2	0.5204(11)	0.25	−0.5070(8)	0.031(3)
V1	0.5	0	0	0.034(5)
V2	0	0.5	0.5	0.031(5)
O1–1	0.475(5)	0.25	0.057(7)	0.048(8)
O1–2	0.017(5)	0.25	0.453(6)	0.044(7)
O2–1	0.270(4)	0.019(5)	0.732(6)	0.03(1)
O2–2	0.773(5)	0.466(5)	−0.229(9)	0.07(2)

lies on the La atomic position. In the bulk reference, the La is strongly displaced from the $0\frac{1}{4}0$ position and, with La–O distances ranging from 2.42 Å and 3.27 Å [19], the oxygen cuboctahedron surrounding La is strongly distorted with 8 first neighbors at an average distance of 2.60 Å and 4 second nearest neighbors at 3.18 Å. In XRD and PEDT refinements performed on our film, the La environment is significantly less distorted than in bulk reference (table 4). Comparing the structures using the COMPSTRU and STRUCTURE RELATIONS tools [31], the La atomic position differs between bulk and thin film by a value of 0.127 Å , 0.094 Å and 0.166 Å for the XRD, PEDT(Pnma) and PEDT ($P2_1/m$) refinements, respectively. Note that in both XRD and PEDT refinements, the La atomic position is robust compared to the oxygen ones. In our case, this reduction of the La displacement compared to the bulk reference can be regarded as a signature of the substrate induced strain amounting up to stresses of 3.5 GPa [13].

4. Conclusion

We exposed an approach targeting the complete structure characterization of a $LaVO_3$ epitaxial thin films from a laboratory x-ray diffraction analysis coupled with a Precession

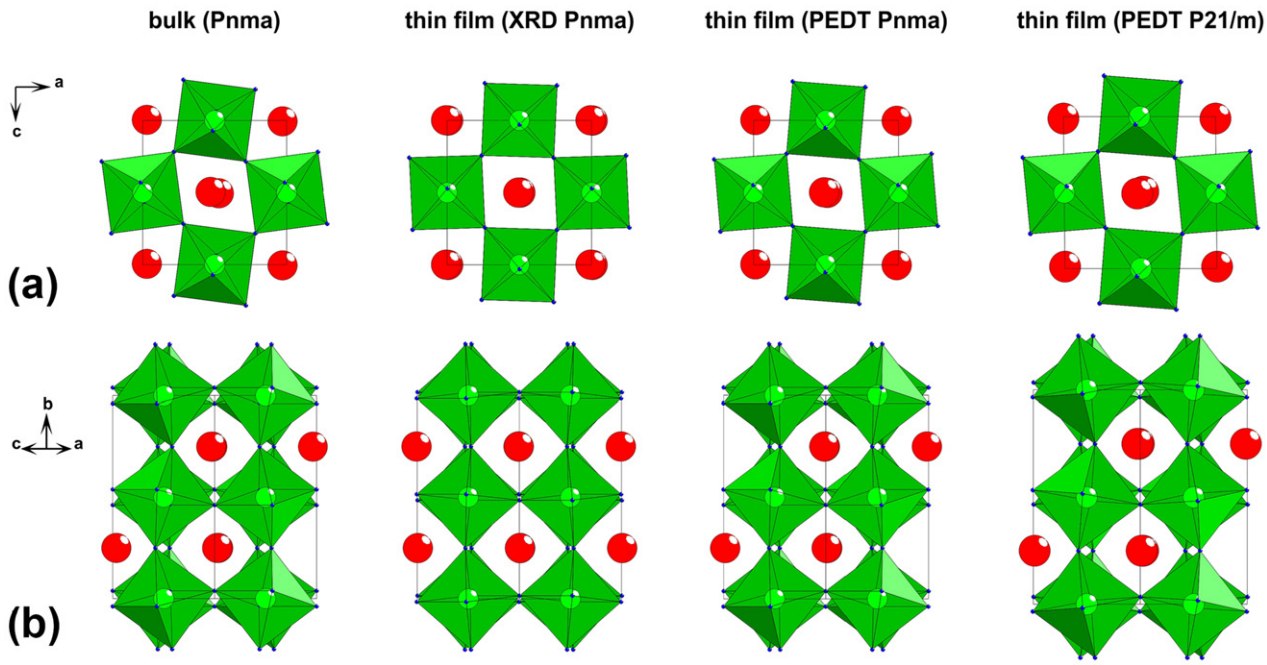

Figure 6. Schematic representation of the structure of bulk LVO (room temperature) [19] and LVO thin films as obtained from XRD and PEDT refinements. (*a*) [0 1 0] projection (*b*) [1 0 1] projection.

Table 4. Selected interatomic distances obtained from the refinement of LVO thin films using XRD and PEDT(Pnma).

	Thin film (XRD)	Thin film (PEDT Pnma)
V1–O1 (x2) (Å)	1.960(9)	1.973(3)
V1–O2 (x2) (Å)	1.97(9)	1.989(19)
V1–O2 (x2) (Å)	1.97(9)	2.000(19)
Average (Å)	1.97	1.99
min La1–O (Å)	2.39(8)	2.47(4)
max La1–O (Å)	3.19(8)	3.15(4)
La1–O 12 (Å)	2.77	2.78
La1–O first 8 (Å)	2.71	2.65
La1–O last 4 (Å)	2.89	3.06

Note: Note that the O–O distances have been constrained to keep an average value of 2.8 Å ± 0.1 Å in the XRD refinement.

Electron Diffraction Tomography measurement. We confirm by XRD the epitaxial relations between the film and the substrate observed by preliminary TEM analysis. We analyze the acquired reciprocal space map and compute them in order to extract the accurate positions and the integrated intensity. We successfully refine the cell parameters in good agreement with our previous study [13] but with higher precision. Finally we proceed to a structure refinement with a fairly good estimation of the atomic positions. Though we obtain realistic atomic positions, the uncertainties are still too high to have sufficient confidence on the refinement results regarding the oxygen positions. Although the necessity of preparing a cross section, the PED tomography is one of the few techniques permitting the rapid acquisition of numerous reflections from a thin film. Here we used this technique to complete our structure analysis of $LaVO_3$ thin film. Such analysis using both XRD and PED is a very promising approach towards accurate cell parameters and structure refinement on epitaxial thin films. However, increasing the number of acquired reflection in XRD would greatly benefit the analysis. Such increase can be achieved by using a synchrotron radiation, a higher incoming flux allow to properly observe the weak reflections in the diffracted pattern of the film and a shorter wavelength overcomes the experimental limitations we encountered with a laboratory experimental set-up. Also the acquisition of the RSM using a 2D detector with a dedicated intensity integration software would be a considerable implement in the reliability of the acquired integrated intensity and thus decrease the reliability factors Robs and wRobs. Even though PED tomography is already a nice complementary tool to laboratory x-ray diffraction for performing structure refinement, in a near future, the treatment of intensities using dynamical theory of electron scattering [32] shall allow to achieve more reliable structure refinement. In a broader perspective, both techniques can be applied to precisely characterize the structure of various epitaxial thin films following our approach.

Acknowledgments

We acknowledge support of the French Agence Nationale de la Recherche (ANR), through the program 'Investissements d'Avenir'(ANR-10-LABX-09-01), LabEx EMC^3 and C'NANO project. The authors thank L Gouleuf for the cross-section preparation and J Lecourt for target preparation. WP and HR thank Dr O Perez (CRISMAT) and Prof S J May (Drexel Univ.) for illuminating discussions and their continuous encouragements during this work. DC and LL acknowlege the Conseil Régional de Basse-Normandie and FEDER for LL's Chair of Excellence financial.

References

[1] Rao C N R and Raveau B 1998 *Transition Metal Oxides* 2nd edn (New York: Wiley)
[2] Imada M, Fujimori A and Tokura Y 1998 *Rev. Mod. Phys.* **70** 1039
[3] Rondinelli J and Spalding N A 2011 *Adv. Mater.* **23** 3363
[4] Dijkkamp D, Venkatesan T, Wu X D, Shaheen S A, Jisrawi N, Min-Lee Y H, McLean W L and Croft M 1987 *Appl. Phys. Lett.* **51** 619
[5] Salvador P A, Haghiri A-M, Mercey B, Hervieu M and Raveau B 1999 *Appl. Phys. Lett.* **75** 2638
[6] Wang J *et al* 2003 *Science* **299** 1719
[7] Tsymbal E Y, Dagotto E R A, Eom C-B and Ramesh R 2012 *Multifunctional Oxide Heterostructures* (Oxford: Oxford University Press)
[8] Moram M and Vickers M 2009 *Rep. Prog. Phys.* **72** 036502
[9] Glazer A 1972 *Acta Crystallogr.* B **28** 33842
[10] Glazer A 1975 *Acta Crystallogr.* A **31** 756
[11] May S J, Kim J-W, Rondinelli J M, Karapetrova E, Spaldin N A, Bhattacharya A and Ryan P J 2010 *Phys. Rev.* B **82** 014110
[12] May S J, Smith C R, Kim J-W, Karapetrova E, Bhattacharya A and Ryan P J 2011 *Phys. Rev.* B **83** 153411
[13] Rotella H, Lüders U, Janolin P-E, Dao V H, Chateigner D, Feyerherm R, Dudzik E and Prellier W 2012 *Phys. Rev.* B **85** 184101
[14] Vailionis A, Oschker B, Siemons W, Houwman E P, Blank D H A, Rijnders G and Koster G 2011 *Phys. Rev.* B **83** 064101
[15] Lu W, Song W D, He K, Chai J, Sun C-J, Chow G-M and Chen J-S 2013 *J. Appl. Phys.* **113** 063901
[16] Vincent R and Midgley P A 1994 *Ultramicroscopy* **53** 271
[17] Boullay P, Dorcet V, Perez O, Grygiel C, Prellier W, Mercey B and Hervieu M 2009 *Phys. Rev.* B **79** 184108
[18] Simon Q, Dorcet V, Boullay P, Demange V, Députier S, Bouquet V and Guilloux-Viry M 2013 *Chem. Mater.* **25** 2793
[19] Bordet P, Chaillout C, Marezio M, Huang Q, Santoro A, Cheong S-W, Takagi H, Oglesby C S and Batlogg B 1993 *J. Solid State Chem.* **106** 253
[20] Kolb U, Gorelik T, Kubel C, Otten M T and Hubert D 2007 *Ultramicroscopy* **107** 507
[21] Hotta Y, Wadati H, Fujimori A, Susaki T and Hwang H Y 2006 *Appl. Phys. Lett.* **89** 251916
[22] Sheets W C, Mercey B and Prellier W 2007 *Appl. Phys. Lett.* **91** 192102
[23] Palatinus L, Klementova M, Drinek V, Jarosova M and Petricek V 2011 *Inorg. Chem.* **50** 3743
[24] Petricek V, Dusek M and Palatinus L 2014 *Z. Kristallogr.* **229** 345
[25] Boullay P, Barrier N and Palatinus L 2013 *Inorg. Chem.* **52** 6127
[26] Chateigner D 2010 *Combined Analysis* (New York: Wiley)
[27] Boullay P *et al* 2011 *Phys. Rev.* B **83** 125403
[28] Lutterotti L 2010 *Nucl. Instrum. Methods Phys. Res.* B **268** 334
[29] Laugier J and Bochu B Celref v3 (www.inpg.fr/LMGP)
[30] Howard C J and Stokes H T 1998 *Acta Crystallogr.* B **54** 782
[31] Tasci E S, de la Flor G, Orobengoa D, Capillas C, Perez-Mato J M and Aroyo M I 2012 *EPJ Web of Conferences* **22** 00009
[32] Palatinus L, Petrícek V and Corrêa C A 2015 *Acta Cryst.* A **71** 235